SAND2012-0079C

Elsevier Editorial System(tm) for Proceedings of the Combustion Institute
Manuscript Draft

Manuscript Number:

Title: Flame chemistry of tetrahydropyran as a model heteroatomic biofuel

Article Type: Research Paper

Keywords: molecular-beam mass spectrometry; kinetics; flat flame; modeling; quantum chemistry

Corresponding Author: Dr. Phillip R. Westmoreland, Ph.D.

Corresponding Author's Institution: North Carolina State University

First Author: Nicole J Labbe, B.S.

Order of Authors: Nicole J Labbe, B.S.; Vikram Seshadri, M.S.; Tina Kasper, Ph.D.; Nils Hansen, Ph.D.; Patrick Patrick Oßwald, Ph.D.; Katharina Kohse-Höinghaus, Ph.D.; Phillip R. Westmoreland, Ph.D.

Abstract: The flame chemistry of tetrahydropyran (THP), a cyclic ether, has been examined using vacuum-ultraviolet (VUV)-photoionization molecular-beam mass spectrometry (PI-MBMS) and flame modeling, motivated by the need to understand and predict the combustion of oxygen-containing, biomass-derived fuels. Species identifications and mole-fraction profiles are presented for a fuel-rich (φ=1.75), laminar premixed THP-oxygen-argon flame at 2.66 kPa (20.0 Torr). Flame species with up to six heavy atoms have been detected. A detailed reaction set was developed for THP combustion that captures relevant features of the THP flame quite well, allowing analysis of the dominant kinetic pathways for THP combustion. Necessary rate coefficients and transport parameters were calculated or were estimated by analogies with a recent cyclohexane reaction set [Li et al., Combust. Flame 158 (2011) 2077-2089], and necessary thermochemical properties were computed using the CBS-QB3 method. Our results show that under the low-pressure conditions, THP destruction is dominated by H-abstraction, and the three resulting THP-yl radicals decompose primarily by β-scissions to two- and four-heavy-atom species that are generally destroyed by β-scission, abstraction, or oxidation.

Flame chemistry of tetrahydropyran as a model heteroatomic biofuel

Nicole J. Labbe,[1] Vikram Seshadri,[2] Tina Kasper,[3] Nils Hansen,[4] Patrick Oßwald,[5]

Katharina Kohse-Höinghaus,[5] and Phillip R. Westmoreland[2#]

[1] University of Massachusetts Amherst, Amherst, MA, USA

[2] North Carolina State University, Raleigh, NC, USA

[3] University of Duisburg-Essen, Germany

[4] Sandia National Laboratories, Livermore, CA, USA

[5] Bielefeld University, Bielefeld, Germany

[#]**Corresponding author:**

Phillip R. Westmoreland

Department of Chemical and Biomolecular Engineering, North Carolina State University, Engineering Building I, Box 7905, Raleigh, NC 27695, USA.

Email: phil.westmoreland@ncsu.edu

Colloquium: Reaction Kinetics

Keywords: molecular-beam mass spectrometry; kinetics; flat flame; modeling; quantum chemistry

Abstract: 171 words

Paper Length (Total word count: 5911 of 6200 maximum):

Main Text:	3432	
Equations:	0	
Nomenclature:	0	
References:	472	[=(25+2)*2.3*7.6]
Tables:	0	
Figures:	2009	[408+329+974+149+149]

Flame chemistry of tetrahydropyran as a model heteroatomic biofuel

Nicole J. Labbe,[1] Vikram Seshadri,[2] Tina Kasper,[3] Nils Hansen,[4] Patrick Oßwald,[5] Katharina Kohse-Hoinghaus,[5] and Phillip R. Westmoreland[2#]

Abstract:

The flame chemistry of tetrahydropyran (THP), a cyclic ether, has been examined using vacuum-ultraviolet (VUV)-photoionization molecular-beam mass spectrometry (PI-MBMS) and flame modeling, motivated by the need to understand and predict the combustion of oxygen-containing, biomass-derived fuels. Species identifications and mole-fraction profiles are presented for a fuel-rich (ϕ=1.75), laminar premixed THP-oxygen-argon flame at 2.66 kPa (20.0 Torr). Flame species with up to six heavy atoms have been detected. A detailed reaction set was developed for THP combustion that captures relevant features of the THP flame quite well, allowing analysis of the dominant kinetic pathways for THP combustion. Necessary rate coefficients and transport parameters were calculated or were estimated by analogies with a recent cyclohexane reaction set [Li et al., *Combust. Flame* 158 (2011) 2077-2089], and necessary thermochemical properties were computed using the CBS-QB3 method. Our results show that under the low-pressure conditions, THP destruction is dominated by H-abstraction, and the three resulting THP-yl radicals decompose primarily by β-scissions to two- and four-heavy-atom species that are generally destroyed by β-scission, abstraction, or oxidation.

1. Introduction

Biofuels are of great interest because they come from renewable sources and can reduce emissions of aromatic hydrocarbons and soot relative to combustion of fossil fuels. However, a recent study has shown that fuels with heteroatoms are apt to form heteroatomic pollutants due to the direct breakdown pathways of the fuel [1-3]. Tetrahydropyran (THP) is the monoether analog of cyclohexane and is the core structure of many sugars and polysaccharides including glucose, a common feedstock for biogenic fuels that have multiple furan and THP-based isomers [4]. These sugars can be pyrolyzed to produce biofuels and bio-derived industrial chemicals, many of which are substituted furans and pyrans [5-6]. Oxidation of THP has been studied in a jet-stirred reactor as a surrogate fuel for diesel models [7] and in shock-tube experiments to understand autoignition of alkanes [8]. THP has been identified as a functional group in several intermediate species in low-temperature oxidation studies of n-alkanes [9].

In the present work, the combustion chemistry of THP is studied to understand the effect of ether linkages on pollutant formation in cyclic fuels, complementing previous studies of the structurally analogous fuels cyclohexane [10], morpholine (1-oxa-4-aza-cyclohexane) [1], and tetrahydrofuran [3]. Photoionization molecular-beam mass spectrometry (PI-MBMS) was conducted on a fuel-rich, laminar flat flame of THP/O_2/Ar to determine mole-fraction profiles. Based on a newly developed THP reaction set, pathways are identified for fuel decomposition and chemical production of potentially harmful emissions.

2. Experiments and Procedures

THP/O_2/25% Ar (Φ=1.75) was burned in a laminar, premixed flat flame at 2.66 kPa (20.0 Torr) and feed mass flux of 0.0443 kg•m^{-2}•s^{-1}. The flame was analyzed using photoionization molecular-beam mass spectrometry (PI-MBMS). Tunable vacuum ultra-violet (VUV) radiation from the Advanced Light Source (ALS) at Lawrence Berkeley National Laboratory allowed single-photon ionization with high

energy resolution. This experimental arrangement has been described in detail previously [11-15] and here will be described only briefly. The flame was stabilized on a 6.0-cm diameter, stainless-steel McKenna-type burner. Gas flows were controlled with calibrated mass flow controllers, and liquid THP was metered by a syringe pump, evaporated, and added to the gas stream. Samples were withdrawn through a 0.40-mm-diameter orifice at the tip of a 40° quartz cone; wall thickness is near 50 μm at the tip. Sampled gas was expanded to ~10^{-4} mbar in the first pumping stage and extracted by a skimmer, forming a molecular beam that passes through the mass spectrometer's (MS) ionization region (~10^{-6} mbar).

Photoionization was by a quasi-continuous photon beam of ~10^{13} photons/s at energies between 8.00 and 17.00 eV, resolved to ~0.05 eV by a 3-m Eagle monochromator. Analysis employed a linear time-of-flight mass spectrometer (TOF-MS) with a mass resolution of $m/\Delta m$=400. Ions were detected by a multichannel plate and integrated with a multichannel scaler with a sensitivity of ~10^{-5}. Mass spectra were collected as functions of the distance h to the burner ("burner scan") or as functions of the photon energy at a fixed distance ("energy scan"). Spectra were corrected for fragmentation and ^{13}C and ^{18}O contributions. Thirty-one species were identified (complete listing in Supplemental Material S1).

The temperature profile used for model calculations combines laser-induced fluorescence (LIF) data with a profile determined from skimmer-chamber pressure. High temperatures were measured with LIF using the frequency-doubled output of an optical parametric oscillator (Continuum Sunlite EX OPO) near 306 nm to excite the OH A–X(0,0) transition. Total fluorescence is monitored with a solar-blind photomultiplier tube with gain set to produce a linear response over the expected range of signals. Accuracy is estimated to be ±150 K in the postflame and reaction zones but is not adequate in the preheat zone, where the OH concentration is much smaller and its concentration gradient is much steeper [16]. Assuming a constant pumping speed, sampling rate through the probe orifice can be expressed as a function of skimmer-chamber pressure and source temperature. LIF data are shifted 2.4

mm to match the skimmer-chamber-pressure temperature profile. The temperature profile is fixed as 450 K at the inlet, post-flame gas temperature is taken from the LIF measurement, and the shape and position of the profile are from the skimmer-chamber-pressure analysis (details in Supplemental Material S2).

3. Model Development and Simulations

A reaction set for THP combustion was developed by analogy to cyclohexane, as shown in Fig. 1. A recent modeling study of cyclohexane combustion at low pressure showed that steady-state, laminar combustion of cyclohexane favors hydrogen-abstraction reactions for cyclohexane destruction [10]. Like cyclohexane, THP is a 6-heavy-atom, saturated ring molecule. Unlike cyclohexane, there are three different distinct hydrogen sites on THP: on the carbons directly adjacent to the ether oxygen (the "2" and "6" carbons), the next neighboring two carbons (the "3" and "5" carbons), and the "4" carbon opposite the oxygen. As a result, there are three distinct routes for THP H-abstraction, each having different reactivities.

For the three resulting THP-yl radicals, decomposition steps to smaller species were assumed to be more important than direct oxidation by oxygen atoms, as had been seen in cyclohexane modeling [10]. THP-yls can undergo β-scissions, breaking the ring to form linear, unsaturated radicals, or they can β-scission a C-H bond, forming unsaturated cyclic molecules (analogous to cyclohexene). The linear radicals preferentially β-scission to a two-heavy-atom molecule (C_2H_x or CH_xO species) plus a four-heavy-atom unsaturated radical that may also undergo further β-scission. Alternatively, the six- or four-heavy-atom radicals may yield unsaturated molecules by β-scission of an H-atom. If an unsaturated cyclic molecule is formed, its allylic H is easily abstracted; β-scission then breaks the ring or creates a doubly unsaturated cyclic molecule (analogous to cyclohexadiene).

A reaction set was constructed for THP combustion using this skeletal mechanism. Reaction rate coefficients and fall-off were derived based on analogous reactions from the cyclohexane model [10] but with Arrhenius pre-exponential factors modified for the proper reaction path degeneracy (RPD). The exception was the three hydrogen abstraction routes from THP to distinguish pathways to the three different THP-yl isomers. For THP+H and THP+CH_3, transition states were calculated using CBS-QB3 with Gaussian09 software [17]; rate coefficients were calculated using canonical transition-state theory and fit to an Arrhenius expression; and rate coefficients for THP+C_2H_3, THP+HCO, and THP+CH_3CO abstractions were then estimated by analogy. Abstraction rate coefficients for THP+O_2, THP+O, THP+OH, and THP+HO_2 were estimated by analogy with cyclohexane reactions. Fall-off for THP-yl decompositions was calculated using unimolecular quantum-RRK theory [18]. The acetylene reaction set from [10] was adapted for the hydrocarbon reactions.

Thermochemistry was calculated theoretically for 22 species in the proposed skeletal mechanism using the complete-basis-set method CBS-QB3. Geometry and frequency calculations were completed using tight convergence criteria. If necessary, transport data were estimated by analogy to molecules of similar structure, size, and molecular weight. The resulting reaction set contains 124 species and 1042 reactions [Supplemental Material S7].

Flame simulations were performed using a modified version of the CHEMKIN-II PREMIX flame code [20-23] including thermal and multi-component diffusion. Experimental temperatures were represented by a smoothed curve (see Fig. 2). Reaction pathways and net reaction rates were analyzed using XSenkPlot [24], adapted from the original code to obtain absolute reaction rates (rather than rates divided by density) and integrated reaction fluxes with respect to distance (rather than time).

4. Results and Discussion

Upon detailed analysis, many predicted features of the flame were in quite good agreement with the data set. Simulations of major-species mole fractions (Fig. 2) show agreement in peak magnitude, shape, and position, useful indicators of model validity. Post-flame mole fractions (beyond about 6 mm) also agree well with the data. No rate coefficients were adjusted to force such a fit; indeed, the model and predictions were developed independently of the experimental mole-fraction analysis. Agreement is presumably the combined result of a generally valid model, accurate measurements, and accuracy of post-flame temperatures.

Precision is generally estimated as <15% for major-species mole-fraction profiles, 30% for species with reliable photoionization cross sections, and approximately a factor of two for intermediates with estimated cross sections. Very close to the burner, the flame is significantly perturbed by the probe, so experimental species mole fractions are only reported at h>1 mm, and quantitative comparisons are not encouraged at less than 2 mm.

The following discussion examines how the THP-flame species are formed and destroyed, revealing sensitivity of minor-species predictions to kinetics of the larger intermediates. Aspects of overall THP flame chemistry are addressed first, followed by discussion of intermediate species and the implications of the kinetics of their formation and destruction.

4.1 THP destruction pathways

Analysis of the simulation is summarized in Fig. 1, showing reaction-arrow line widths scaled proportionally to the integrated reaction fluxes. The thickest lines thus show the major routes of fuel combustion. THP itself is consumed by H-abstraction from the three distinct positions in the proportions THP-2-yl:THP-3-yl:THP-4-yl::10:9:5. These THP-yls are mainly consumed by β-scission of C-C or C-O bonds, opening the ring to form additional mass-85 isomers that β-scission to C_2H_4 or CH_2O plus a

four-heavy-atom radical. From the latter radicals, β-scission of C-C or C-O bonds forms C_2H_3, C_2H_4, HCO, and CH_2O, while β-scission of C-H bonds forms 1,3-butadiene or acrolein.

By comparison, β-scission of C-H bonds causes relatively minor THP-yl destruction channels, forming 3,4-dihydro-2H-pyran and 3,6-dihydro-2H-pyran, the two possible cyclohexene-like C_5H_8O isomers (mass 84). In addition, several open-chain isomers may also contribute to mass 84. The dihydropyran species can undergo H-abstraction to form cyclic mass-83 species, which may β-scission to ring mass-83 species or to form the pyran diene at mass 82.

The number of isomers expected to contribute at mass 85, 84, 83, and 82 makes experimental identification and quantification difficult, yet the limited comparisons for these species and the good comparisons for smaller species lend support to the model's validity. Eleven mass-85 species and five mass-84 species may contribute, and they could not be resolved experimentally. Model results for THP-diene (mass 82) were only a factor of two higher than the data, which is acceptably within the range of uncertainty.

4.2 Kinetics of THP-yl decomposition intermediates

Four-heavy-atom intermediates. It was possible to identify and provide estimates for the mole fractions of some species featuring four heavy atoms that result from the further fuel breakdown. From the skeletal mechanism in Fig. 1, key species in this mass range include $\bullet CH_2CH_2CH{=}O$ and $\bullet CH_2OCH{=}CH_2$ at mass 57, acrolein ($CH_2{=}CH\text{-}CH{=}O$) at mass 56, $\bullet CH_2CH_2CH{=}CH_2$ (C_4H_7, mass 55), and 1,3-butadiene ($CH_2{=}CHCH{=}CH_2$) at mass 54. All these four-heavy-atom segments of the original ring structure preserve the sequence of heavy atoms, coming from decomposition rather than molecular-weight-growth processes.

The mass-57 radicals could not be resolved, but mass 56 was identified as acrolein and is predicted reasonably well by the model (Fig. 3h). The peak magnitude is predicted well, although the

predicted peak is shifted from the experimental profile by approximately 2 mm away from the burner.

A signal at mass 55 was also observed, but species of molecular formulas C_4H_7 and C_3H_3O could not be distinguished. To propose what mass 55 could be, the model predictions for mass-55 species were compared. The only C_4 species in the decomposition routes, C_4H_7, was predicted to be dominant over all other mass-55 species. The model prediction of mass 55 was quite good, supporting its origin as being THP-yl decomposition. Additional indirect support comes from the good prediction of 1,3-butadiene, which is formed primarily from C_4H_7 by decomposition or H-abstraction. Butadiene is predicted to be about 50% higher than that which was observed experimentally (Fig. 3g).

Two-heavy-atom intermediates. The skeletal fuel-decomposition mechanism leads to a number of stable and radical species with two heavy atoms (bottom of Fig. 1), including C_2H_2, C_2H_3, C_2H_4, HCO, and CH_2O. They result from more than one pathway, though.

Experimental and predicted mole-fraction profiles for C_2H_4 and C_2H_2 are presented in Fig. 3c. The simulation shows good agreement for C_2H_4, matching profile magnitude, position, and shape well. Analysis of the reaction rates (Fig. 4) show that C_2H_4 is produced almost entirely from the THP-yl decomposition routes. The same is true for C_2H_4 production in cyclohexane flames (from cyclohexyl). Of the multiple routes for C_2H_4 formation, the principal formation paths are $\bullet OCHCH_2CH_2 \rightarrow C_2H_4+HCO$, $\bullet CH_2CH_2CH_2CH_2CHO \rightarrow C_2H_4+\bullet CH_2CH_2CHO$, $\bullet CH_2CH_2OCH_2CHCH_2 \rightarrow C_2H_4+\bullet OCH_2CHCH_2$, and $\bullet CH_2CH_2CH_2OCHCH_2 \rightarrow C_2H_4+\bullet CH_2OCHCH_2$. The prediction for the C_2H_2 mole-fraction profile captures its peak position and profile shape quite accurately, and its peak magnitude agrees within expected uncertainty. It is produced by decomposition of C_2H_3, which is formed through the THP-yl decomposition paths.

By comparison, CH_2O appears over-predicted by a factor of three, and HCO is under-predicted by a factor of five, although the peak positions and shapes are in good agreement (Fig. 3b). The

inconsistencies are most likely due to greater HCO calibration uncertainty or its being converted too fast in the model, as many radicals abstract its H.

In the THP flame, CH_2O is predominantly formed directly from the THP-yl decomposition reaction steps, based on the model analysis presented in Fig. 5, where net rates of CH_2O formation and destruction are graphed for the main contributors in the THP flame. CH_2O is predominantly formed from decomposition of six-heavy-atom radicals $\bullet CH_2OCH_2CH_2CH{=}CH_2$ and $\bullet OCH_2CH_2CH_2CH{=}CH_2$ and a four-heavy-atom radical $\bullet CH_2OCH{=}CH_2$ that are from the THP-yl decomposition sequence. The $C_2H_3+O_2 \rightleftarrows HCO+CH_2O$ and $\rightleftarrows H+CO+CH_2O$ reactions contribute as well, where C_2H_3 and its precursor C_2H_4 (via $C_2H_4+R \rightleftarrows C_2H_3+RH$, where R is a radical) come mainly from THP-yl decomposition. CH_2O is destroyed by H-abstraction, mainly by H and OH, so accuracy of those radicals' predictions will affect the relative CH_2O and HCO.

A key insight is that the prediction of CH_2O formation in the THP flame is not strongly related to predictive capability for C_1 and C_2 oxidation reactions. Methyl is not the main source of CH_2O here, unlike CH_4 flames where $CH_3+O \rightleftarrows H+CH_2O$ predominates. The THP situation is more like that of cyclohexane flames [10], where C_2H_3 and C_2H_4 are produced as cyclohexyl ring-decomposition products, but for THP, CH_2O and HCO are also produced. Thus, uncertainty in the predicted CH_2O and HCO profiles may be attributed to the more complex decomposition chemistry of the heterocyclic THP fuel.

4.3 Other intermediates and pathways

As discussed above, species with an even number of heavy atoms can form from THP through abstractions and β-scissions. By contrast, species with an odd number of heavy atoms can form from a mix of decomposition and chemically activated oxidation and radical-addition and combination

reactions.

CH_3 and CH_4. The very good predictions of CH_3 and CH_4 (Fig. 3a) strongly support the model because of the complex routes by which CH_3 is formed. The positions of the maxima are reproduced well by the model; also, the general shapes of the profiles are in reasonable agreement with the experiment. Prediction of the CH_4 mole-fraction profile is excellent, the onset of CH_3 is well-described in shape and magnitude, and the CH_3 peak and high-temperature behavior are acceptable.

CH_3 chemistry is the key to both profiles, as the CH_4 is mainly from reversible $CH_3+RH \rightleftarrows CH_4+R$ abstractions. At $h<4.5$ mm where CH_3 formation chemistry dominates its profile, the three main formation reactions are $CH_2CHO(+M) \rightarrow CH_3+CO(+M)$ from Senosiain *et al.* [25], *i*-$C_4H_5+H \rightarrow CH_3+C_3H_3$, and $CH_2CHO+H \rightarrow CH_3+HCO$. The C/H/O reactants result from channels in the THP-yl decomposition sequences (Fig. 1). CH_2CHO ("vinoxy") is predicted to be from decomposition of 4-pentenal and vinylallyl ether, the two mono-oxygen analogs of 1,5-hexadiene. In turn, these two oxygenates are formed by secondary decomposition channels of the linear radicals formed from ring-opening of THP-2-yl and THP-3-yl. The *i*-C_4H_5 is formed by H-abstraction from 1,3-butadiene, a direct product of the THP-4-yl decomposition sequence. Some CH_3 destruction occurs in this region, mainly H-abstraction from the decomposition-generated HCO.

The CH_3 profile at $h>4.5$ mm is dominated by the higher-temperature formation reactions of $C_2H_4+O \rightleftarrows CH_3+HCO$ and production from CH_4 and by destruction through CH_3+O and OH. Note that because CH_4 is formed from and destroyed to CH_3, the accurately predicted CH_4 profile depends on correct rate coefficients, temperature, and concentrations of CH_3, RH, and R.

C_3H_x compounds. Profiles of propargyl (C_3H_3), propyne and allene (C_3H_4 isomers), allyl (C_3H_5), and propene (C_3H_6) are presented in Fig. 3d-e. These species are significant in part because C_3H_3 is a precursor to phenyl and benzene, which are thought to be precursors of polycyclic aromatic hydrocarbons and soot.

C_3H_3 has a peak mole fraction of $8 \cdot 10^{-4}$ in the ϕ=1.75 THP flame, approximately half of the peak observed in a ϕ=2.0 cyclohexane flame [10]. The presence of the oxygen atom in THP reduces the possibilities of forming a three-carbon chain in the fuel breakdown and reduces the yield of C_3H_3. The predicted propargyl mole fraction is somewhat higher than the experimental profile (within a factor of two) and it is accurate with regard to profile peak position and shape, as shown in Fig. 3d. Its formation is dominated by i-$C_4H_5+H \rightleftarrows CH_3+C_3H_3$, which is also important for CH_3 formation.

Mole-fraction profiles of allene and propyne are both predicted well by the model (Fig. 3e). Reaction analysis shows that propyne formation is dominated by H-catalyzed interconversion from allene, the abstraction C_3H_3+HCO, and $C_2H_2+CH_3$. Allene formation, on the other hand, has significant contributions from abstraction and decomposition reactions of allyl, the only C_3H_x isomer formed directly from THP decomposition. The model is within a factor of two (lower) than the experimental data.

Propene has a peak mole fraction of 0.003. The prediction is lower than the data by a factor of two. In the model, C_3H_6 is almost entirely formed by H-atom combination with allyl.

C_4H_x compounds. In addition to 1,3-butadiene, discussed earlier, C_4H_2, C_4H_4, and C_4H_8 were measured, and their mole-fraction profiles are presented in Fig. 3f-g. Like 1,3-butadiene, these species are generally derived from C_4H_7. C_4H_8 is formed dominantly from C_4H_7+H and C_4H_7+HCO, although the model under-predicts C_4H_8 by a factor of three. H-abstraction from 1,3-butadiene yields the C_4H_5 isomers, and vinylacetylene, C_4H_4, is formed primarily from hydrogen abstraction from C_4H_5. Its mole-fraction profile is predicted quite well, including peak magnitude and position. The contribution of C_4H_2 is over-predicted by slightly more than a factor of two. C_4H_2 is predicted to be formed via hydrogen abstraction from C_4H_3 species.

Ketene and benzene. Ketene CH_2CO is formed predominantly from CH_2CHO and from C_2H_2+OH. Prediction of its mole-fraction profile is within a factor of two (Fig. 3h) of the experimental

data, but its peak is at lower *h* than in the data.

Benzene is detected in the flame, formed by molecular-weight growth because unlike cyclohexane, THP cannot dehydrogenate to a phenyl ring. The predicted maximum of the benzene mole fraction, $8 \cdot 10^{-5}$, is within a factor of two of the experimental data (Fig. 3h). Upon analysis, *i*-C_4H_5+C_2H_2→fulvene(+H→benzene+H), C_3H_3+C_3H_3→benzene, and *n*-C_4H_5+C_2H_2→benzene+H appear to be the dominant formation routes.

5. Conclusions

THP combustion has been analyzed in a low-pressure premixed flat flame at ϕ=1.75. From VUV-PI-MBMS measurements, 31 species with up to six heavy atoms are quantified. A newly developed kinetic mechanism for THP starts from recent modeling of cyclohexane combustion and adds rate coefficients and thermochemistry from quantum chemistry. This model predicts the general flame structure well. Analyzing the predictions shows that THP consumption in the flame is by abstractions of the three different H atoms in THP, followed by logical sequences of decomposition steps from the THP-yl radicals. These radicals then β-scission to six-, four-, and two-heavy-atom species by a logical sequence. Other species are formed by decomposition and oxidation of these intermediates. Although little molecular-weight growth was observed, benzene is produced, and routes are identified to produce it.

THP is studied here as a small C/H/O-containing model biofuel with the aim of contributing to the understanding of the mechanistic pathways for THP combustion and the formation of potential pollutants. The reaction set and kinetic pathways identified in this study will aid design of efficient, low-polluting combustors. THP is an ether variant of cyclohexane and the non-nitrogen equivalent of morpholine, and the present flame data and predictions provide insights into mechanistic similarities and differences from these other fuels.

Acknowledgements

This work was supported in part by the U.S. Department of Energy (P.R.W.) under contract DE-FG02-91ER14192 and by the Department of Defense (DoD) through a National Defense Science & Engineering Graduate Fellowship (N.J.L.). This work was partially supported by the National Center for Supercomputing Applications under grant number TG-CTS090056 using the Cobalt supercomputer (N.J.L. and P.R.W.). NH is supported in part by the U.S. Department of Energy, Office of Basic Energy Sciences under the Energy Frontier Research Center for Combustion Science (Grant No. DE-SC0001198). Sandia is a multi-program laboratory operated by Sandia Corporation, a Lockheed Martin Company, for the National Nuclear Security Administration under contract DE-AC04-94-AL85000. PI-MBMS measurements were performed within the "Flame Team" collaboration at the Advanced Light Source, Lawrence Berkeley National Laboratory, which is supported by the US DOE/BES under DE-AC02-05CH11231. The experiments have benefitted from the able support of technicians, doctoral students, and postdocs, including Wenjun Li and Bin Yang.

References

[1] A. Lucassen, N. Labbe, P.R. Westmoreland, K. Kohse-Höinghaus, *Combust. Flame* 158 (2011) 1647-1666.

[2] K. Kohse-Höinghaus, P. Oßwald, T. A. Cool, T. Kasper, N. Hansen, F. Qi, C. K. Westbrook, P. R. Westmoreland*, Angew. Chem. Int. Ed.* 49 (2010) 3572-3597.

[3] T. Kasper, A. Lucassen, A. W. Jasper, W. Li, P. R. Westmoreland, K. Kohse-Höinghaus, B. Yang, J. Wang, T. A. Cool, N. Hansen, *Z. Phys. Chem.* **225** (2011) 1237-1270.

[4] A. Osmont, L. Catoire, P. Escot Bocanegra, I. Gökalp, B. Thollas, J. A. Kozinski, *Combust. Flame* 157 (2010) 1230-1234.

[5] K. Sipila, E. Kuoppala, L. Fagernas, A. Oasmaa, *Biomass and Bioenergy* 14 (1998) 103-113.

[6] R. M. West, E. L. Kunkes, D. A. Simonetti, J. A. Dumesic, *Catalysis Today* 147 (2009) 115-125.

[7] M. H. Hichem, P. A. Glaude, O. Herbinet, F. Battin-Leclerc, *Combust. Flame* 156 (2009) 2129-2144.

[8] P. Dagaut, M. McGuinness, J. M. Simmie, M. Cathonnet, *Combust. Sci. and Tech.* 129 (1997) 1-16.

[9] O. Herbinet, S. Bax, P. A. Glaude, V. Carre, F. Battin-Leclerc, *Fuel* 90 (2011) 528-535.

[10] W. Li, M. E. Law, P. R. Westmoreland, T. Kasper, N. Hansen, K. Kohse-Höinghaus, *Combust. Flame* 158 (2011) 2077-2089.

[11] T. A. Cool, K. Nakajima, T. A. Mostefaoui, F. Qi, A. McIlroy, P. R. Westmoreland, M. E. Law, L. Poisson, D. S. Peterka, and M. Ahmed, *J. Chem. Phys.* **119** (2003) 8356-8365.

[12] T. A. Cool, A. McIlroy, P. R. Westmoreland, M. Ahmed, D. S. Peterka, L. Poisson, *Rev. Sci. Instrum.* **76** (2005) 094102-1 to 094102-7.

[13] T. A. Cool, K. Nakajima, C. A. Taatjes, A. McIlroy, P. R. Westmoreland, M. E. Law, A. Morel, *Proc. Combust. Inst.* **30** (2005) 1681–1688.

[14] C. A. Taatjes, N. Hansen, D. L. Osborn, K. Kohse-Höinghaus, T. A. Cool, P. R. Westmoreland, *Phys. Chem. Chem. Phys.* **10** (2008) 20-34.

[15] N. Hansen, T. A. Cool, P. R. Westmoreland, K. Kohse-Höinghaus, *Prog. Energy Combust. Sci.* **35** (2009) 168-191.

[16] N. Hansen, M.R. Harper, W.H. Green, *Phys. Chem. Chem Phys.* **13** (2011) 20262-20274

[17] M. J. Frisch, G. W. Trucks, H. B. Schlegel, G. E. Scuseria, M. A. Robb, J. R. Cheeseman, G. Scalmani, V. Barone, B. Mennucci, G. A. Petersson, H. Nakatsuji, M. Caricato, X. Li, H. P. Hratchian, A. F. Izmaylov, J. Bloino, G. Zheng, J. L. Sonnenberg, M. Hada, M. Ehara, K. Toyota, R. Fukuda, J. Hasegawa, M. Ishida, T. Nakajima, Y. Honda, O. Kitao, H. Nakai, T. Vreven, J. A. Montgomery, Jr., J. E. Peralta, F. Ogliaro, M. Bearpark, J. J. Heyd, E. Brothers, K. N. Kudin, V.

N. Staroverov, R. Kobayashi, J. Normand, K. Raghavachari, A. Rendell, J. C. Burant, S. S. Iyengar, J. Tomasi, M. Cossi, N. Rega, J. M. Millam, M. Klene, J. E. Knox, J. B. Cross, V. Bakken, C. Adamo, J. Jaramillo, R. Gomperts, R. E. Stratmann, O. Yazyev, A. J. Austin, R. Cammi, C. Pomelli, J. W. Ochterski, R. L. Martin, K. Morokuma, V. G. Zakrzewski, G. A. Voth, P. Salvador, J. J. Dannenberg, S. Dapprich, A. D. Daniels, Ö. Farkas, J. B. Foresman, J. V. Ortiz, J. Cioslowski, and D. J. Fox, *Gaussian 09, Revision A.1*, Gaussian, Inc., Wallingford CT, 2009.

[18] P. R. Westmoreland, J. B. Howard, J. P. Longwell, A. M. Dean, *AIChE J.* 32 (1986) 1971-1979.

[19] W. Li, P.R. Westmoreland, N. Hansen, B. Yang, T. A. Cool, K. Kohse-Höinghaus [in preparation].

[20] R. J. Kee, J. A. Miller, T. H. Jefferson, *CHEMKIN II version 2.5: A General-Purpose, Problem-Independent, Transportable, Fortran Chemical Kinetics Code Package*, SAND80-8003, Sandia National Laboratories, Livermore, California, 1980. Modification of CHEMKIN version 3.9, 1992.

[21] R. J. Kee, G. Dixon-Lewis, J. Warnatz, M. E. Coltrin, J. A. Miller, *A Fortran Computer Package for the Evaluation of Gas-Phase, Multicomponent Transport Properties*, SAND87-8246, Sandia National Laboratories, Livermore, California, 1986. Modification of TRANLIB version 1.6, 1990.

[22] R. J. Kee, J. F. Grcar, M. D. Smooke, J. A. Miller, *A Fortran Program for Modeling Steady Laminar One-Dimensional Premixed Flames*, SAND85-8240, Sandia National Laboratories, Livermore, California, 1985. Modification of PREMIX version 2.5, 1991.

[23] R.J. Kee, F.M. Rupley, J.A. Miller, *The Chemkin Thermodynamic Database*, SAND87-8215, Sandia National Laboratories, Livermore, California, 1987.

[24] D. R. F. Burgess Jr., *Program XSenkplot*, National Institute of Science and Technology, Gaithersburg MD, 1997.

[25] J. P. Senosiain, S. J. Klippenstein, J. A. Miller. *J. Phys. Chem. A* **109** (2005) 6045-6055.

Figures:

Figure 1:

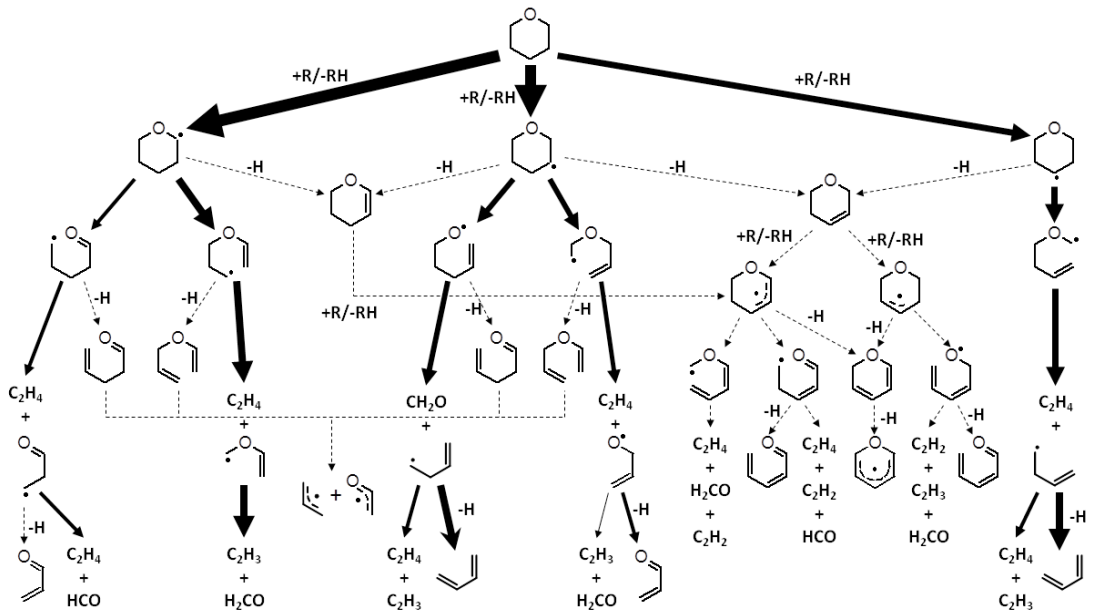

Figure 2:

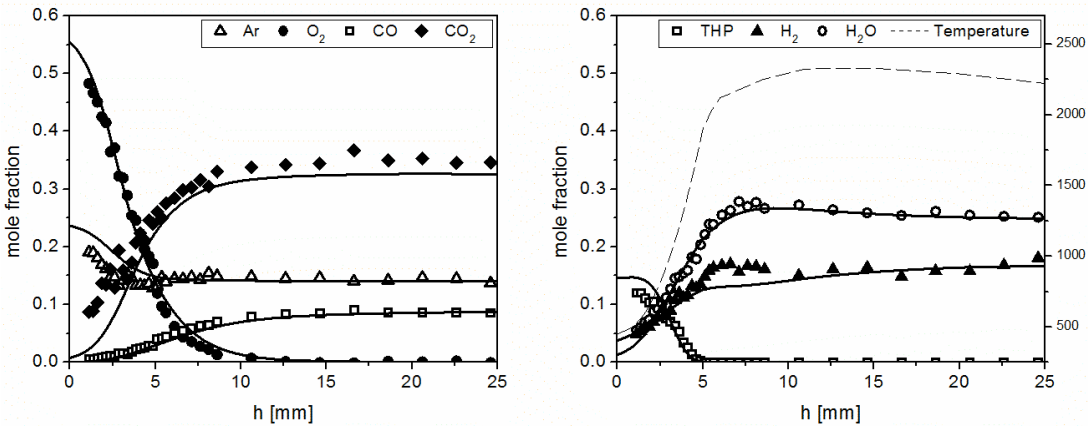

Figure 3:

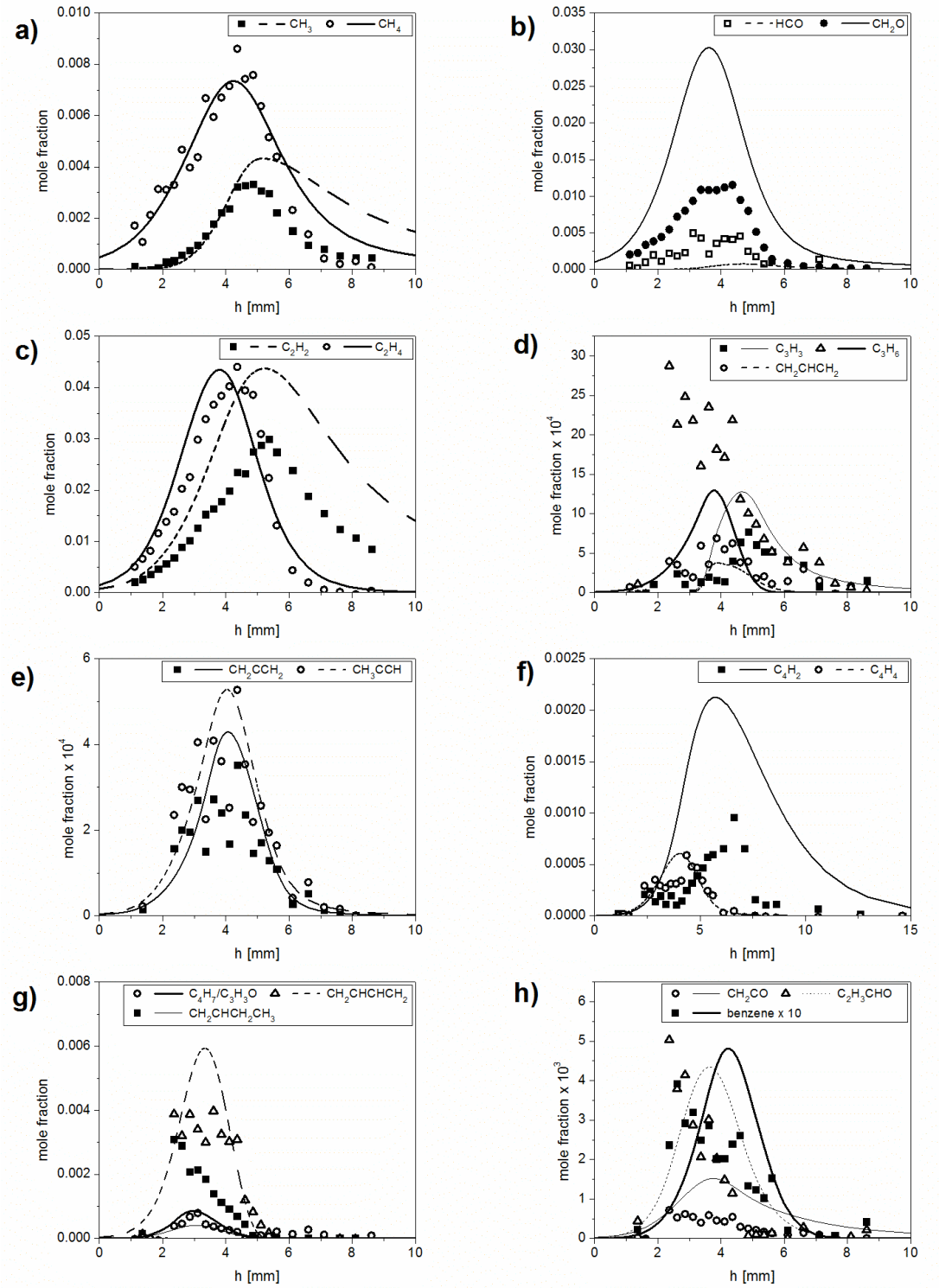
a)
CH3
CH4
mole fraction
h [mm]
b)
HCO
CH2O
mole fraction
h [mm]
c)
C2H2
C2H4
mole fraction
h [mm]
d)
C3H3
C3H6
CH2CHCH2
mole fraction x 10^4
h [mm]
e)
CH2CCH2
CH3CCH
mole fraction x 10^4
h [mm]
f)
C4H2
C4H4
mole fraction
h [mm]
g)
C4H7/C3H3O
CH2CHCHCH2
CH2CHCH2CH3
mole fraction
h [mm]
h)
CH2CO
C2H3CHO
benzene x 10
mole fraction x 10^3
h [mm]

Figure 4:

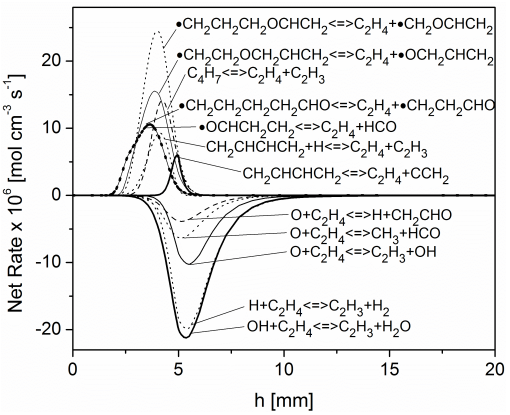

Figure 5:

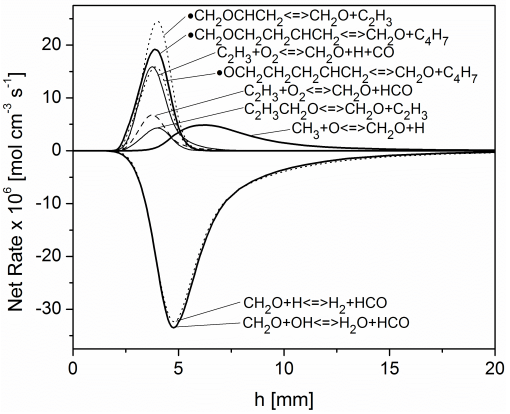

Figure Captions

Figure 1: Skeletal reaction-mechanism diagram for THP flame.

Figure 2: Major-species mole-fraction profiles: (left) Ar, O_2, CO, CO_2; (right) THP, H_2, H_2O, temperature. Symbols indicate experimental data (data for the first 1.0 mm have been omitted due to perturbation); lines are from flame model.

Figure 3: Mole-fraction profiles of intermediate species including a) CH_3 and CH_4, b) HCO and CH_2O, c) C_2H_2 and C_2H_4, d) $C_3H_{5\text{-}7}$ e) C_3H_4s, f) C_4H_2 and C_4H_4, g) $C_4H_{6\text{-}8}$, and C_3H_3O, and h) CH_2CO, C_2H_3CHO, and benzene. Symbols indicate experimental data (data for the first 1.0 mm have been omitted due to perturbation); lines are from flame model.

Figure 4: Reaction-rate diagram for C_2H_4.

Figure 5: Reaction-rate diagram for CH_2O.

List of Supplemental Material

S1: Species and calibration factors

S2: Experimental temperature profile

S3: THP rate constants

S4: Input file for CHEMKIN Premix simulation

S5: Thermodynamic database for model

S6: Transport database for model

S7: THP mechanism file

Supplemental Material

Click here to download Supplemental Material: 12THP_SupplementalData.pdf